

RESEARCH PAPER

Characterization and Antimicrobial Activity of Hydrogel SA-g-P(AAc-co-Am) Leded with Zinc Oxide Nanoparticles

Zainab Hashim Khudhair¹, Qusay K. Mojar Alshamusi², Makarim A. Mahdi², and Layth S. Jasim^{2*}

¹ Department of Chemistry, College of Sciences for Women, Babylon University, Hilla, Iraq

² Department of Chemistry, College of Education, University of Al-Qadisiyah, Al-Qadisiyah, Iraq

ARTICLE INFO

Article History:

Received 25 May 2024

Accepted 19 September 2024

Published 01 October 2024

Keywords:

Adsorption

Equilibrium

Hydrogel

Kinetic

Sodium Alginate

Zinc oxide nanoparticles

ABSTRACT

The study focused on the characterization and biological activity of odium alginate graft poly (acrylic acid-co-acrylamide) Hydrogel (SA-g-P(AAc-co-Am)) impregnated with Zinc Oxide nanoparticles. Using FTIR, FE-SEM, TEM, and XRD techniques, various features were analyzed including the structural composition, surface morphology, and particle size. FTIR analysis showed active groups' displacement after adsorption of ZnO nanoparticles, while FE-SEM unveiled a porous structure useful for adsorption. TEM images suggested uniform ZnO nanoparticles distribution, while XRD revealed an amorphous nature of the hydrogel. The biological activity against *Staphyococcus aureus*, *Escherichia coli*, and *Aspergillums Niger* was studied, with higher inhibition observed in the latter as the concentration of ZnO nanoparticles increased. However, differences in biological response were noticed, attributed to the varying nature of each organism.

How to cite this article

Khudhair Z., Alshamusi Q., Mahdi M., Jasim L. Characterization and Antimicrobial Activity of Hydrogel SA-g-P(AAc-co-Am) Leded with Zinc Oxide Nanoparticles. J Nanostruct, 2024; 14(4):1097-1106. DOI: 10.22052/JNS.2024.04.011

INTRODUCTION

Adsorption is one of the most successful technologies for purification and separation processes, and it is employed on such a huge scale in our manufacturing economy and in our daily lives that adsorption procedures are found in almost every industry today [1, 2]. According to literature studies, adsorption on porous surfaces represents an effective method for the removal of organic and inorganic contaminants from air and distilled water [3-12]. Polymeric nanoparticles have gotten a lot of attention as nano carriers because of their capacity to protect the bioactive ingredient while also allowing it to be released in a regulated manner [13, 14]. Researchers

have been paying close attention to polymeric nanoparticles because of their stability and ease of surface modification, and Nano composite materials combine the features of inorganic and biopolymer materials [15-19]. In the fields of biology and medicine, cytostatic potential of nanoparticles of zinc oxide (ZnO-NPs) towards cancerous cells, their potential against microbes as well as fungi, their capacity to expedite curing wound, their application in bio-imaging owing to chemiluminescent characteristics of nanoparticles along with their potential against diabetes widely studied [9-13]. Sodium Alginate has sparked a lot of interest in the pharmaceutical industry because of its promising qualities like biodegradability,

* Corresponding Author Email: layth.alhayder@gmail.com



biocompatibility, and antibacterial characteristics Tumors and viruses , Because of these intriguing qualities, sodium alginate along with its byproducts find uses for different pharmaceutical purposes [18, 20-23].

Objective of this study is to investigate and analyze the characteristics of SA-g-P(AAc-co-Am) hydrogel post-loading by zinc oxide nanoparticles, including morphological, structural, and functional properties. Additionally, the study aims to evaluate the biological activity of the prepared composite against various bacterial and fungal pathogens, examining the potential inhibitory effects on their growth.

MATERIALS AND METHODS

Chemicals and materials

The materials utilized in the study were obtained from a variety of suppliers. Acrylamide was secured from Himedia, located in India. Potassium persulfate (KPS, employed as initiator), was procured from Merck (Germany). The N, N'- methylene bisacrylamide (NMBA), a

multifunctional crosslinker, procured from Fluka (Germany). Alpha Chemika supplied sodium chloride while ZnO purchased from Sigma-Aldrich, Germany.

Preparation of SA-g-P(AAc-co-Am)

SA-g-P(AAc-co-Am) was prepared utilizing a series of solutions. Initially, a 1% v/v solution of AAC was prepared. Concurrently, 1.0 g of sodium alginate was dissolved in 60 mL of AAC, stirred for 50 min (45°C). KPS solution was then created by dissolving 0.4 g of it in 4 mL of distilled water, while an Acrylamide (AM) solution was formed by dissolving 4 g of AM in 4 mL of distilled water. Additionally, a linking solution was prepared from MBA by dissolving its 0.1g in 4 mL water. Subsequently, KPS solution added to sodium alginate solution (in drop-way manner) while stirring, followed by addition of AM solution, while stirr for 5 min. The MBA (N,N-Methylene-Bisacrylamide) was then added while stirring and infusing nitrogen gas for 3 min. This prepared solution was then transferred to water bath (50°C)

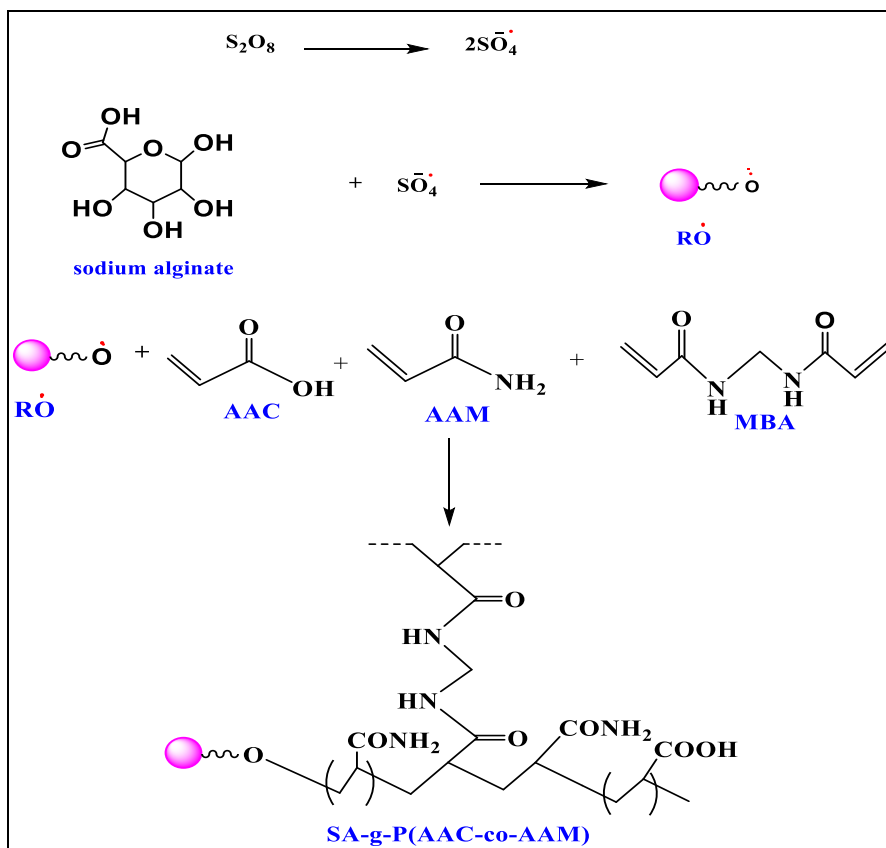


Fig. 1. Scheme of SA-g-P(AAc-co-Am) synthesis

for 3 h. With distilled water, resulting polymer then purified followed by drying at 60°C [14]. The equations for hydrogel synthesis are visually represented in Fig. 1.

Loading of zinc nanoparticles

The equilibrium time for nano zinc oxide loading was determined, keeping all parameters including temperature, pressure, solution concentration, and surface weight constant, thereby making time the sole variable. Ten samples of 10ml zinc oxide solution, each with a concentration of 100ppm, were prepared. These samples were individually placed in a 25ml conical flask, to each of which 0.05g of the adsorbent surface was added. Following this, they were placed in a shaker and samples were extracted at various time intervals (1-240 minutes). These samples were then centrifuged at a speed of 6000 rpm for 15 minutes. Each sample's absorbance was quantified at a peak wavelength of $\lambda_{max}=370nm$. From these absorbance values, an equilibrium time of 120 minutes was inferred.

Antimicrobial Activity

Three different solutions of nano Zinc Oxide (ZnO-NPs) were prepared at different concentrations (1-15 mg/mL) and adsorbed onto the surface of CH-g-P(AA-co-Am) using both distilled water and DMSO solvent. Biological activity was evaluated for each solution over a range of 5-15 hours to determine optimal adsorption timing against two pathogenic bacteria strains: Staphylococcus aureus (a Gram-positive Bacteria) and Escherichia coli (a Gram-negative Bacteria). Additionally, a strain

of the fungus Aspergillus Niger was studied to determine the inhibitory impact of this composite on the growth of these organisms.

RESULTS AND DISCUSSION

Characterization

FTIR

The FTIR analysis of SA-g-P(AAc-co-Am) depicted in Fig. 2 illustrates the interaction of the hydroxyl group (3320 cm^{-1}) having group of amine (3423 cm^{-1}), resulting from existing H-bond between them. Band at (2928 cm^{-1}) corroborates presence of R-groups, peak at (1618 cm^{-1}) highlight $-C=O$ of amide group. However, peak at (1643 cm^{-1}) signifies $-C=O$ of $-COOH$ group. Peak (1314 cm^{-1}) corresponds to carbon-nitrogen bond. Owing to the hydrogen binding to active groups on hydrogel surface, these groups' absorption packs are displaced and reduced post adsorption of zinc oxide [24, 25]. The radiation spectrum indicated that ZnO adsorption onto surface resulted in the displacement and diminution of ionic groups' adsorption peaks on the hydrogel surface. Peaks within the range of $520-750\text{ cm}^{-1}$ represent the vibrational stretching of ZnO nanoparticles, as metal oxides typically manifest in regions below 1000 cm^{-1} . This signifies that ZnO nanoparticles are present and are intermingled with the hydrogel [26-36].

FE-SEM

FE-SEM of SA-g-P(AAc-co-Am) revealed spongy structures, indicating good adsorption sites and a shell-like composite membrane structure. This

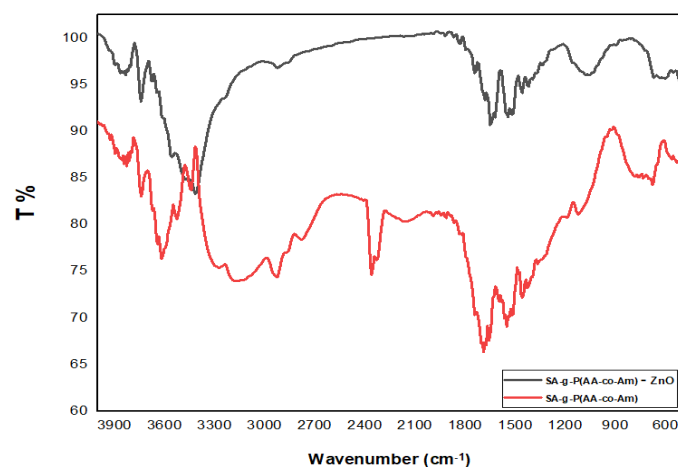


Fig. 2. FTIR for hydrogel pre and post adsorption of ZnO nanoparticles

porous interconnection is attributed to attachment of polymer chains via some cross-linker, thereby enhancing swelling of hydrogel. Post-adsorption, surface findings depict increased smoothness of the prepared surface (Fig. 3). This is a consequence of the surface pores being filled with zinc oxide particles, resulting in a crusty layer that could be single or multi-layered. The presence of zinc oxide particles on the surface confirms the occurrence of the process [37, 38].

TEM

TEM was applied to the Hydrogel SA-g-P(AA-

co-Am) before and after loading it with zinc oxide. Fig. 4 illustrates different magnifications of the surface. These images distinctly suggest the presence of uniformly distributed, small granules organized in a regular clumping pattern, attributed to the sodium alginate matrix. Fig. 4 reveals the Hydrogel SA-g-P(AA-co-Am) covered by heterogeneous, spherically shaped nanoparticles that are uniformly distributed zinc oxide (ZnO-NPs) particles [39].

The structural properties of the composition, crystal size, and interplanar distances of the hydrogel were investigated via X-ray diffraction

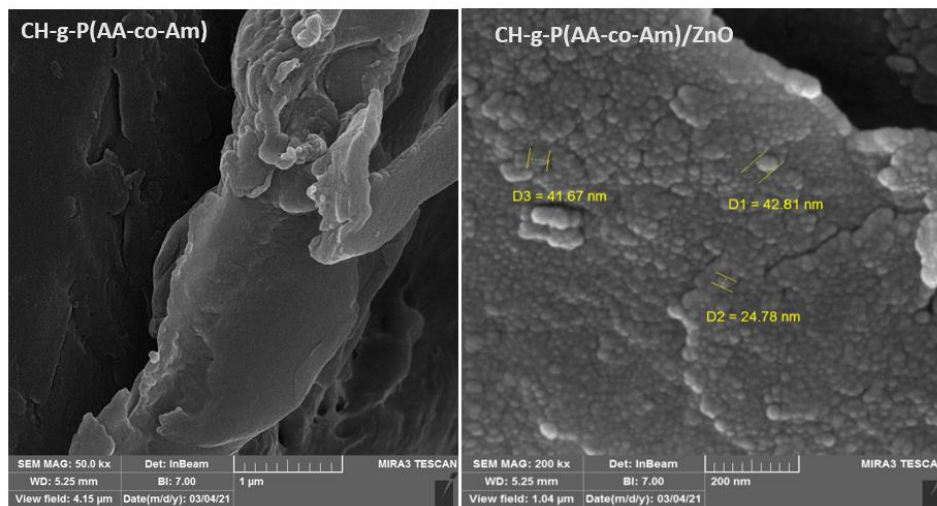


Fig. 3. FESEM for SA-g-P(AAc-co-Am) before and after Loading of zinc oxide nanoparticles

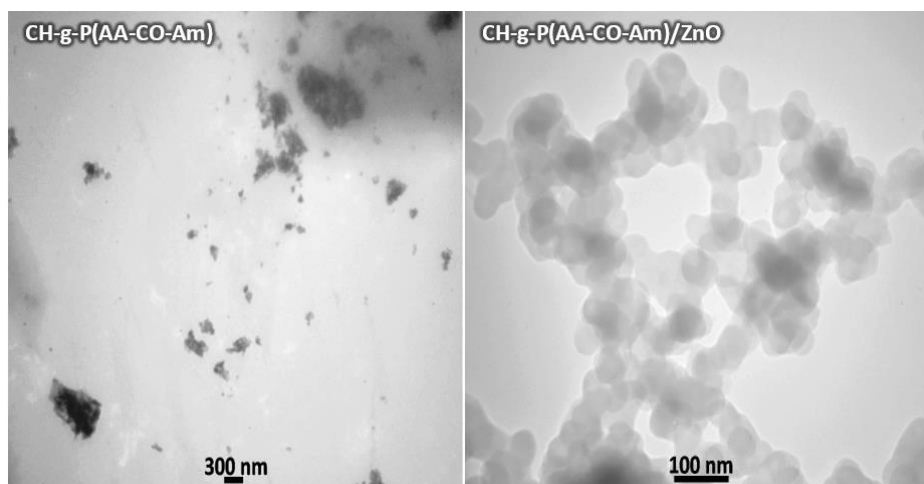


Fig. 4. TEM image obtained from Transmission Electron Microscopy displaying the composite surface before and after adsorption of nano-sized ZnO particles

(XRD). Broad band depicted in Fig. 5 suggests that the hydrogel possesses an amorphous structure[40-42].

Debye-Scherrer expression used for calculating size of crystal for prepared hydrogel:

$$D = \frac{k \lambda}{\beta \cos \theta} \quad (1)$$

Since d represents the spacing amongst the plane of crystallinity, n referring to an integer

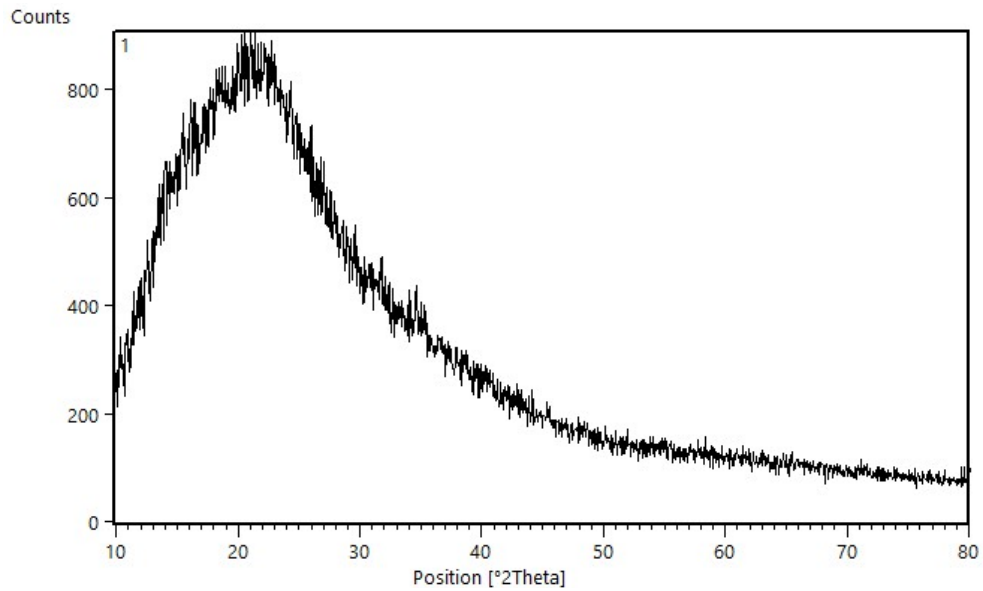


Fig. 5. X-ray diffraction of hydrogel

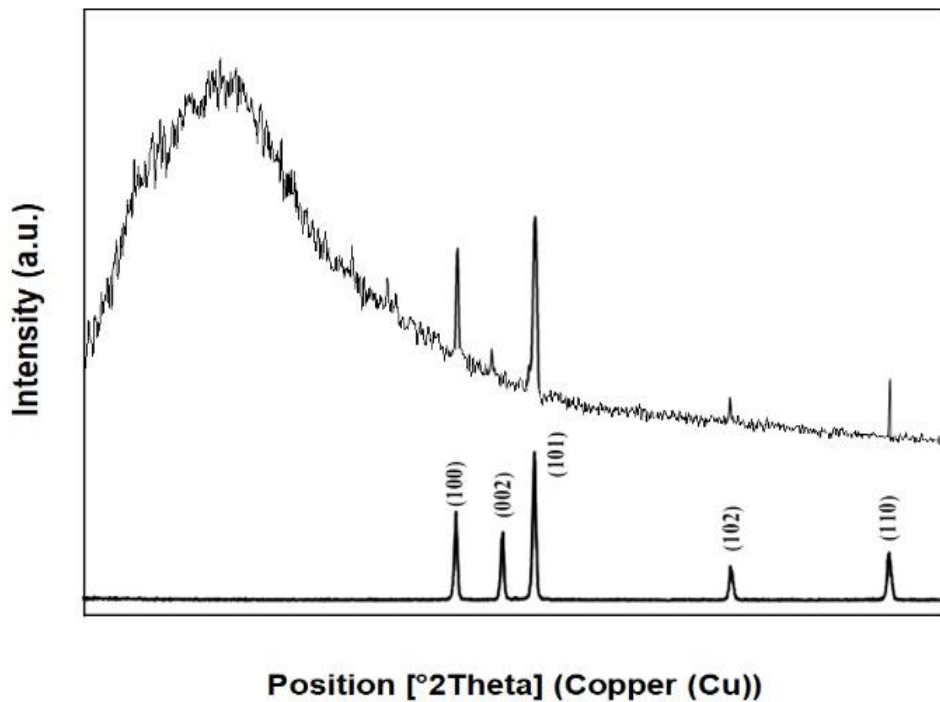


Fig. 6. X-ray diffraction of Hydrogel after zinc oxide adsorption

(1,2,3,), Table 1 shows diffraction angel, values of d-spacing, as well as relative intensity of the beams and Hydrogel[43].

After loading zinc oxide, the results showed a clear adsorption ZnO on the surface of the Hydrogel, as shown in the Fig. 6 through the visible

Table 1. Diffraction angles, distance of interlayer, index of Miller, as well as X-ray diffraction spectrum intensity for hydrogel

Peak	2Theta (deg)	Θ	d-spacing (Å°)	FWHM	Intensity (I/I ₀) %	Sheet Size D(nm)	lattice strain
1	.064 21	10.532	4.217	0.587	100	14.4	0.013
2	16.08	8.04	5.50	0.56	84	15	0.0174
3	31.735	15.867	2.818	0.310	55	27.8	0.0048
4	34.617	17.308	2.591	0.333	47	26.1	0.0047

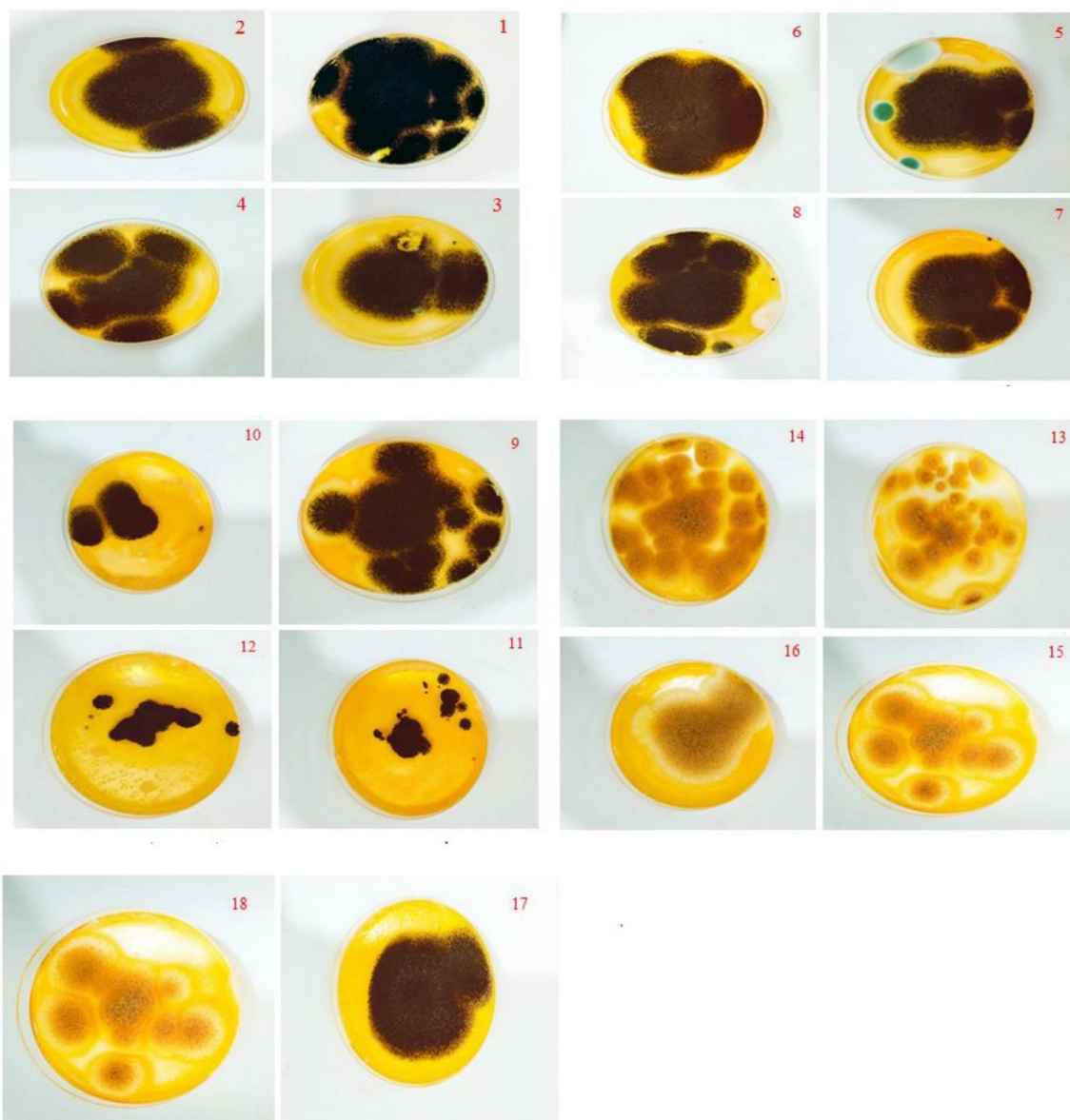


Fig. 7. Effect of composite of SA-g-P(AAc-co-Am) at different concentration (mg/mL) of ZnO in inhibiting Aspergillus

Table 2. The range of inhibition diameters for *E.coli*, *S.aureus* and *Aspergillus nige* at different concentrations and times.

No.	Anti-bacterial Activity		Anti-fungal Activity
	<i>E.coli</i>	<i>S.aureus</i>	<i>Aspergillus niger</i>
1	R	R	10
2	R	R	27.5
3	R	R	30
4	R	1	32.5
5	25.0	25	37.5
6	17.5	5	12
7	35	10	22.5
8	35	15	25
9	R	R	25
10	R	R	50
11	R	R	65
12	R	R	75
13	50	10	37
14	14	5	30
15	23	20	25
16	5	20	25
17	25	23	25
18	R	R	32.5

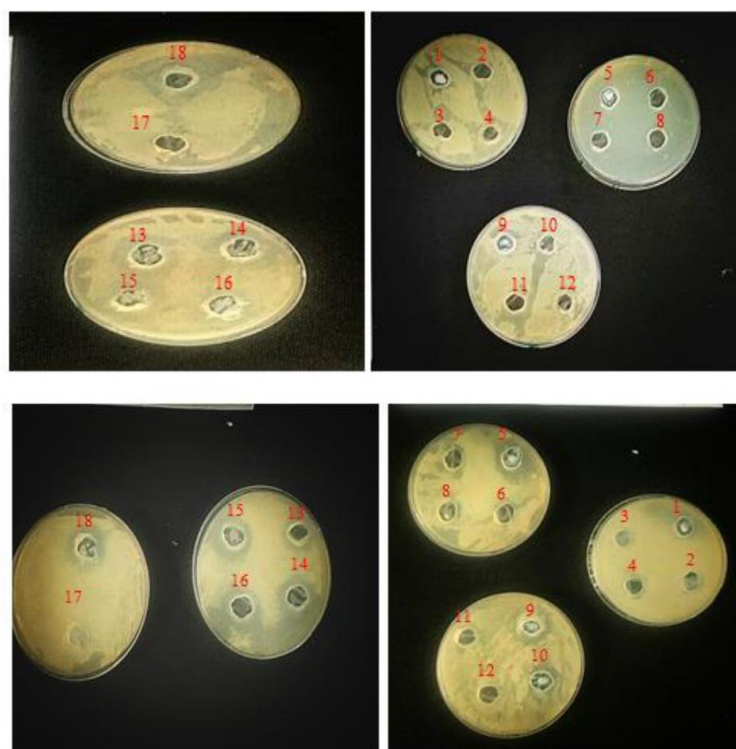


Fig. 8. Effect of composite of SA-g-P(AAc-co-Am) at different concentration (mg/mL) of ZnO in inhibiting bacteria

Table 3. compounds used in biological activity with different concentrations and times

Compound	No.	Time (hr.)	Conc.(mg/mL)
ZnO in solvent H ₂ O	1	-	1
SA-g-P(AAc-co-Am)/ ZnO in solvent H ₂ O	2	5	1
SA-g-P(AAc-co-Am)/ ZnO in solvent H ₂ O	3	10	1
SA-g-P(AAc-co-Am)/ ZnO in solvent H ₂ O	4	15	1
ZnO in solvent H ₂ O	5	-	5
SA-g-P(AAc-co-Am)/ ZnO in solvent H ₂ O	6	5	5
SA-g-P(AAc-co-Am)/ ZnO in solvent H ₂ O	7	10	5
SA-g-P(AAc-co-Am)/ ZnO in solvent H ₂ O	8	15	5
ZnO in solvent H ₂ O	9	-	15
SA-g-P(AAc-co-Am)/ ZnO in solvent H ₂ O	10	5	15
SA-g-P(AAc-co-Am)/ ZnO in solvent H ₂ O	11	10	15
SA-g-P(AAc-co-Am)/ ZnO in solvent H ₂ O	12	15	15
ZnO in solvent DMSO	13	-	1
SA-g-P(AAc-co-Am)/ ZnO in solvent DMSO	15	1	1
SA-g-P(AAc-co-Am)/ ZnO in solvent DMSO	16	1	5
SA-g-P(AAc-co-Am) in solvent DMSO	17	-	
SA-g-P(AAc-co-Am) in solvent DMSO	18	-	

beams at 2 θ equal to (25.2, 35.3, 38.3, 55.4, 65.3), which belong to the zinc oxide[44].

Biological Activity

The inhibitory diameter (in mm) was measured for both bacterial and fungal types, where the symbol (R) indicates resistance of bacteria and fungi to inhibition. Findings revealed that inhibition of fungus *Aspergillus Niger* increased with both an increase in concentration of Zinc Oxide solution and time (Fig. 7). As for the bacteria *S.aureus* and *E.coli*, both types of bacteria showed resistance to inhibition at a concentration of 1mg/mL of Zinc Oxide solution (Fig. 8). Upon increasing the concentration to 5mg/mL, inhibition of bacteria and fungi was observed because increasing the concentration leads to enhanced activity due to partial solubility in distilled water. However, upon increasing the concentration to 15mg/mL, the bacteria showed minimal inhibition compared to the fungi, which showed good inhibition. This could be attributed to the differences in the biological nature of each organism. When DMSO solvent was used at concentrations of 1-5mg/mL, these concentrations showed inhibitory effect on

bacteria and fungi due to the high solubility of ZnO in DMSO, which damages the outer envelope of the bacteria and thereby inhibits them[45-47].

CONCLUSION

Based on the FTIR analysis, it can be concluded that various functional groups, including hydroxyl, amine, and carbonyl groups, are present in the hydrogel and exhibit changes upon zinc oxide absorption, indicating active interactions between the hydrogel and zinc oxide nanoparticles. SEM and TEM analyses reveal a porous structure of the hydrogel, which provides ample sites for zinc oxide adsorption, and confirm the successful loading of zinc oxide particles on the hydrogel surface. XRD data indicate an amorphous structure of hydrogel, with additional peaks after ZnO loading pointing to the successful incorporation of ZnO on hydrogel surface. The biological activity analysis suggests that the zinc oxide-loaded hydrogel exhibits considerable antimicrobial activity, with a stronger inhibitory effect on fungi than bacteria. This effect appears to be concentration and time-dependent. Overall, the zinc oxide-loaded SA-g-P(AAc-co-Am) hydrogel presents promising potential for

biomedical and biological applications due to its excellent absorption properties and antimicrobial activity.

CONFLICT OF INTEREST

The authors declare that there is no conflict of interests regarding the publication of this manuscript.

REFERENCES

1. Adsorption Processes for Water Treatment and Purification. Springer International Publishing; 2017.
2. Al-Ghouti MA, Da'ana DA. Guidelines for the use and interpretation of adsorption isotherm models: A review. *J Hazard Mater.* 2020;393:122383.
3. Radia ND, Essa SM, Aljeboree AM, Abed Jawad M. Evaluation of the Adsorption Efficiency of Biopolymer Hydrogel Nanocomposite/Nanoclay in Wastewater Dye Removal. *Asian Journal of Water, Environment and Pollution.* 2024;21(4):47-54.
4. Batool M, Javed T, Wasim M, Zafar S, Din MI. Exploring the usability of Cedrus deodara sawdust for decontamination of wastewater containing crystal violet dye. *Desalination and Water Treatment.* 2021;224:433-448.
5. Ghzal Q, Javed T, Batool M. Potential of easily prepared low-cost rice husk biochar and burnt clay composite for the removal of methylene blue dye from contaminated water. *Environmental Science: Water Research and Technology.* 2023;9(11):2925-2941.
6. Majeed HJ, Idrees TJ, Mahdi MA, Abed MJ, Batool M, Yousefi SR, et al. Synthesis and application of novel sodium carboxy methyl cellulose-g-poly acrylic acid carbon dots hydrogel nanocomposite (NaCMC-g-PAAC/ CDs) for adsorptive removal of malachite green dye. *Desalination and Water Treatment.* 2024;320:100822.
7. Bukhari A, Javed T, Haider MN. Adsorptive exclusion of crystal violet dye from wastewater by using fish scales as an adsorbent. *J Dispersion Sci Technol.* 2022;44(11):2081-2092.
8. Imran MS, Javed T, Areej I, Haider MN. Sequestration of crystal violet dye from wastewater using low-cost coconut husk as a potential adsorbent. *Water Sci Technol.* 2022;85(8):2295-2317.
9. Urooj H, Javed T, Taj MB, Nouman Haider M. Adsorption of crystal violet dye from wastewater on Phyllanthus emblica fruit (PEF) powder: kinetic and thermodynamic. *Int J Environ Anal Chem.* 2023;104(19):7474-7499.
10. Arshad R, Javed T, Thumma A. Exploring the efficiency of sodium alginate beads and Cedrus deodara sawdust for adsorptive removal of crystal violet dye. *J Dispersion Sci Technol.* 2023;45(12):2330-2343.
11. Javed T, Thumma A, Uddin AN, Akhter R, Babar Taj M, Zafar S, et al. Batch adsorption study of Congo Red dye using unmodified Azadirachta indica leaves: isotherms and kinetics. *Water Practice and Technology.* 2024;19(2):546-566.
12. Rehman H, Javed T, Thumma A, Uddin AN, Singh N, Baig MM, et al. Potential of easily available low-cost raw cotton for the elimination of methylene blue dye from polluted water. *Desalination and Water Treatment.* 2024;318:100319.
13. Artech Pujana M, Pérez-Álvarez L, Cesteros Iturbe LC, Katime I. pH-sensitive chitosan-folate nanogels crosslinked with biocompatible dicarboxylic acids. *Eur Polym J.* 2014;61:215-225.
14. Jabbar FA, Jasim LS, Sahib IJ. Characterization, modelling, and kinetics studies of the adsorption of phenol from aqueous solutions onto [ZnO/P(AA-CA)] composite as an adsorbate surface. *AIP Conference Proceedings: AIP Publishing;* 2023. p. 040002.
15. Gupta D, Singh D, Kothiyal NC, Saini AK, Singh VP, Pathania D. Synthesis of chitosan-g-poly(acrylamide)/ZnS nanocomposite for controlled drug delivery and antimicrobial activity. *Int J Biol Macromol.* 2015;74:547-557.
16. Valian M, Salavati-Niasari M, Ganduh SH, Abdulsahib WK, Mahdi MA, Jasim LS. Sol-gel auto-combustion synthesis of a novel chitosan/Ho₂Ti₂O₇ nanocomposite and its characterization for photocatalytic degradation of organic pollutant in wastewater under visible illumination. *Int J Hydrogen Energy.* 2022;47(49):21146-21159.
17. Mahdi MA, Jasim LS, Ranjeh M, Masjedi-Arani M, Salavati-Niasari M. Improved pechini sol-gel fabrication of Li₂B₄O₇/NiO/Ni₃(BO₃)₂ nanocomposites to advanced photocatalytic performance. *Arabian Journal of Chemistry.* 2022;15(5):103768.
18. Kareem NS, Mohammed SA, Abed MJ, Aneed AH, Kamal HM, Zahid NI, et al. New macrocycles incorporating glycolipids via copper-catalyzed triazole coupling. *J Carbohydr Chem.* 2022;41(1):1-17.
19. Mahdi MA, Oroumi G, Samimi F, Dawi EA, Abed MJ, Alzaidy AH, et al. Tailoring the innovative Lu₂CrMnO₆ double perovskite nanostructure as an efficient electrode materials for electrochemical hydrogen storage application. *Journal of Energy Storage.* 2024;88:111660.
20. Naushad M, Ahamad T, Al-Sheetan KM. Development of a polymeric nanocomposite as a high performance adsorbent for Pb(II) removal from water medium: Equilibrium, kinetic and antimicrobial activity. *J Hazard Mater.* 2021;407:124816.
21. Dan S, Banivaheeb S, Hashemipour H, kalantari M. Synthesis, characterization and absorption study of chitosan-g-poly(acrylamide-co-itaconic acid) hydrogel. *Polym Bull.* 2020;78(4):1887-1907.
22. Functional Chitosan. Springer Singapore; 2019.
23. Kapitel I 23. *Analytica posteriora: De Gruyter;* 1993. p. 841-852.
24. Lalita, Singh AP, Sharma RK. Selective sorption of Fe(II) ions over Cu(II) and Cr(VI) ions by cross-linked graft copolymers of chitosan with acrylic acid and binary vinyl monomer mixtures. *Int J Biol Macromol.* 2017;105:1202-1212.
25. Makhado E, Pandey S, Modibane KD, Kang M, Hato MJ. Sequestration of methylene blue dye using sodium alginate poly(acrylic acid)@ZnO hydrogel nanocomposite: Kinetic, Isotherm, and Thermodynamic Investigations. *Int J Biol Macromol.* 2020;162:60-73.
26. Gutha Y, Pathak JL, Zhang W, Zhang Y, Jiao X. Antibacterial and wound healing properties of chitosan/poly(vinyl alcohol)/zinc oxide beads (CS/PVA/ZnO). *Int J Biol Macromol.* 2017;103:234-241.
27. Thakur S, Arotiba OA. Synthesis, swelling and adsorption studies of a pH-responsive sodium alginate-poly(acrylic acid) superabsorbent hydrogel. *Polym Bull.* 2018;75(10):4587-4606.
28. Shah A, Arjunan A, Manning G, Zakharova J, Andraulaki I, Batool M. The effect of dose, settling time, shelf life,

- storage temperature and extractant on *Moringa oleifera* Lam. protein coagulation efficiency. *Environmental Nanotechnology, Monitoring and Management*. 2024;21:100919.
29. Batool M, Haider MN, Javed T. Applications of Spectroscopic Techniques for Characterization of Polymer Nanocomposite: A Review. *Journal of Inorganic and Organometallic Polymers and Materials*. 2022;32(12):4478-4503.
30. Batool M, Abid MA, Javed T, Haider MN. Applications of biodegradable polymers and ceramics for bone regeneration: a mini-review. *International Journal of Polymeric Materials and Polymeric Biomaterials*. 2024;74(1):39-53.
31. Zhang M, Zhong J, Song Z, Xu Q, Chen Y, Zhang Z. Regulatory mechanisms and potential therapeutic targets in precancerous lesions of gastric cancer: A comprehensive review. *Biomedicine and Pharmacotherapy*. 2024;177:117068.
32. Jamdar M, Monsef R, Ganduh SH, Dawi EA, Jasim LS, Salavati-Niasari M. Unraveling the potential of sonochemically achieved $\text{DyMnO}_3/\text{Dy}_2\text{O}_3$ nanocomposites as highly efficient visible-light-driven photocatalysts in decolorization of organic contamination. *Ecotoxicology and Environmental Safety*. 2024;269:115801.
33. Atyaa AI, Radhy ND, Jasim LS. Synthesis and Characterization of Graphene Oxide/Hydrogel Composites and Their Applications to Adsorptive Removal Congo Red from Aqueous Solution. *Journal of Physics: Conference Series*. 2019;1234(1):012095.
34. Rahimkhoei V, Alzaidy AH, Abed MJ, Rashki S, Salavati-Niasari M. Advances in inorganic nanoparticles-based drug delivery in targeted breast cancer theranostics. *Advances in Colloid and Interface Science*. 2024;329:103204.
35. Razavi FS, Mahdi MA, Ghanbari D, Dawi EA, Abed MJ, Ganduh SH, et al. Fabrication and design of four-component $\text{Bi}_2\text{S}_3/\text{CuFe}_2\text{O}_4/\text{CuO}/\text{Cu}_2\text{O}$ nanocomposite as new active materials for high performance electrochemical hydrogen storage application. *Journal of Energy Storage*. 2024;94:112493.
36. The value of two onset determination of anti-H.pylori IgM antibody in patients with dyspepsia in Iraq. *International Journal of Pharmaceutical Research*. 2020;12(02).
37. Patel SR, Patel MP. Green and facile preparation of ultrasonic wave-assisted chitosan-g-poly-(AA/DAMPB)/ Fe_3O_4 composite hydrogel for sequestration of reactive black 5 dye. *Polym Bull*. 2021;79(5):3193-3217.
38. Zabihi E, Babaei A, Shahrampour D, Arab-Bafrani Z, Mirshahidi KS, Majidi HJ. Facile and rapid in-situ synthesis of chitosan-ZnO nano-hybrids applicable in medical purposes; a novel combination of biomineralization, ultrasound, and bio-safe morphology-conducting agent. *Int J Biol Macromol*. 2019;131:107-116.
39. Jamdar M, Heydariyan Z, Alzaidy AH, Dawi EA, Salavati-Niasari M. Eco-friendly auto-combustion synthesis and characterization of $\text{SmMnO}_3/\text{Sm}_2\text{O}_3/\text{Mn}_2\text{O}_3$ nanocomposites in the presence of saccharides and their application as photocatalyst for degradation of water-soluble organic pollutants. *Arabian Journal of Chemistry*. 2023;16(12):105342.
40. Qayoom M, Dar GN. Crystallite Size and Compressive Lattice Strain in NiFe_2O_4 Nanoparticles as Calculated in Terms of Various Models: Influence of Annealing Temperature. *Int J Self-Propag High-Temp Synth*. 2020;29(4):213-219.
41. Bayati-Komitaki N, Ganduh SH, Alzaidy AH, Salavati-Niasari M. A comprehensive review of Co3O nanostructures in cancer: Synthesis, characterization, reactive oxygen species mechanisms, and therapeutic applications. *Biomedicine and Pharmacotherapy*. 2024;180:117457.
42. Hosseini M, Ghanbari M, Alzaidy AH, Dawi EA, Mahdi MA, Jasim LS, et al. Synthesis and characterization of $\text{Fe}_2\text{SiO}_4/\text{Fe}_2\text{O}_3/\text{g-C}_3\text{N}_4$ ternary heterojunction photocatalyst with enhanced photocatalytic activity under visible light. *Int J Hydrogen Energy*. 2024;60:1370-1382.
43. Trikkaliotis DG, Christoforidis AK, Mitropoulos AC, Kyzas GZ. Adsorption of copper ions onto chitosan/poly(vinyl alcohol) beads functionalized with poly(ethylene glycol). *Carbohydr Polym*. 2020;234:115890.
44. Kushwaha CS, Singh P, Abbas NS, Shukla SK. Self-activating zinc oxide encapsulated polyaniline-grafted chitosan composite for potentiometric urea sensor. *Journal of Materials Science: Materials in Electronics*. 2020;31(14):11887-11896.
45. Khashan KS, Sulaiman GM, Hussain SA, Marzoog TR, Jabir MS. Synthesis, Characterization and Evaluation of Anti-bacterial, Anti-parasitic and Anti-cancer Activities of Aluminum-Doped Zinc Oxide Nanoparticles. *Journal of Inorganic and Organometallic Polymers and Materials*. 2020;30(9):3677-3693.
46. Kaur T, Putatunda C, Vyas A, Kumar G. Zinc oxide nanoparticles inhibit bacterial biofilm formation via altering cell membrane permeability. *Preparative Biochemistry and Biotechnology*. 2020;51(4):309-319.
47. The value of iron supplementation to children with *Helicobacter pylori* infection in Iraq: a cross-sectional study. *International Journal of Pharmaceutical Research*. 2020;12(02).